

# Search for associations containing young stars (SACY):

## II. Chemical abundances of stars in 11 young Associations in the Solar neighborhood <sup>★</sup>

P. Viana Almeida<sup>1,2,6</sup>, N.C. Santos<sup>1,6</sup>, C. Melo<sup>3</sup>, M. Ammler-von Eiff<sup>4</sup>, C. A. O. Torres<sup>5</sup>, G.R. Quast<sup>5</sup>, J.F. Gameiro<sup>1,6</sup>,  
and M. Sterzik<sup>2</sup>

<sup>1</sup> Centro de Astrofísica, Universidade do Porto, Rua das Estrelas, 4150-762 Porto, Portugal

<sup>2</sup> ESO, Alonso de Cordova 3107, Casilla 19001, Vitacura, Santiago, Chile  
e-mail: palmeida@eso.org

<sup>3</sup> ESO, Karl-Schwarzschild-Str.2, 85748 Garching bei München, Germany

<sup>4</sup> Centro de Astronomia e Astrofísica da Universidade de Lisboa, Observatório Astronómico de Lisboa, Tapada da Ajuda, 1349-018 Lisboa, Portugal

<sup>5</sup> Laboratório Nacional de Astrofísica/ MCT, Rua Estados Unidos 154, 37504-364 Itajubá (MG), Brazil

<sup>6</sup> Departamento de Matemática Aplicada, Faculdade de Ciências da Universidade do Porto, Portugal

Preprint online version: October 26, 2018

### ABSTRACT

The recently discovered coeval, moving groups of young stellar objects in the solar neighborhood represent invaluable laboratories to study recent star formation and to search for high metallicity stars which can be included in future exo-planet surveys. In this study we derived through an uniform and homogeneous method stellar atmospheric parameters and abundances for iron, silicon and nickel in 63 Post T-Tauri Stars from 11 nearby young associations. We further compare the results with two different pre-main sequence (PMS) and main sequence (MS) star populations. The stellar atmospheric parameters and the abundances presented here were derived using the equivalent width of individual lines in the stellar spectra through the excitation/ionization equilibrium of iron. Moreover, we compared the observed Balmer lines with synthetic profiles calculated for model atmospheres with a different line formation code. We found that the synthetic profiles agree reasonably well with the observed profiles, although the Balmer lines of many stars are substantially filled-in, probably by chromospheric emission. Solar metallicity is found to be a common trend on all the nearby young associations studied. The low abundance dispersion within each association strengthens the idea that the origin of these nearby young associations is related to the nearby Star Forming regions (SFR). Abundances of elements other than iron are consistent with previous results on Main Sequence stars in the solar neighborhood. The chemical characterization of the members of the newly found nearby young associations, performed in this study and intended to proceed in subsequent works, is essential for understanding and testing the context of local star formation and the evolutionary history of the galaxy.

**Key words.** stars: pre-main sequence – stars: formation – stars: abundances – open clusters and associations – stars: fundamental parameters

### 1. INTRODUCTION

For many years the canonical star-forming regions (such as Taurus, Rho-Oph, Sco-Cen complex, for instance) were the closest places to study astrophysical issues related to the (local and recent) star-formation process.

The confirmation by Kastner et al. (1997) of an early suggestion made by Gregorio-Hetem (1992) that a small group of young stars around TW Hydra would form a loose association sharing common characteristics such as age, distance, x-ray emission level and radial velocities, showed that young stars can be found at a much closer distance than previously thought.

Since then, a dozen of young nearby associations have been identified (see reviews by Zuckermann & Song 2004; Torres et al. 2003b; Torres et al. 2008). These associations are valuable laboratories to study recent star formation in the solar neighborhood.

Thanks to the proximity, they may yield precious clues that can lead to a better understanding of a wide variety of current open issues concerning the formation and evolution of planetary systems.

Because typical ages of these groups match the timescales for disk dispersal (*e.g.* Spangler et al. 2001) and planet formation (Pollack et al. 1996) they constitute interesting targets for exoplanet searches.

As previous studies strongly suggest (*e.g.* Gonzalez 1997; Gonzalez et al. 2001; Santos et al. 2001; Santos et al. 2004; Santos et al. 2005; Fisher & Valenti 2005), planet-host stars may display a higher metal content. Consequently it becomes relevant to look for a high metallicity sample among young stars, such as these Post-T Tauri stars (PTTS), in order to better focus future planetary search projects.

In this context, it is important to carry out a chemical characterization of the newly-found loose associations and compare them with the typical stellar population, both the older MS (Sousa et al. 2008) and the younger PMS (James et al. 2006; Santos et al. 2008) found near the Sun. That comparison

<sup>★</sup> Based on observations collected with the UVES spectrograph at the VLT/UT2 8.2-m Kueyen Telescope (ESO run ID. 079.C-0556(A)) at the Paranal Observatory, Chile

could lead to a better understanding of the origin of the stellar population in the solar neighborhood.

In this study we present stellar parameters and chemical abundances for 63 PTTS in 11 young nearby associations, being them the AB Doradus (AB Dor) (Zuckermann et al. 2004c; Torres et al. 2008), Argus (Torres et al. 2008),  $\beta$  Pictoris (Zuckermann et al. 2001a; Song et al. 2003; Torres et al. 2006; Torres et al. 2008), Carina, Columba (Torres et al. 2008),  $\varepsilon$  Chamaeleon (Barrado y Navascués 1998; Mamajek et al. 2000; Torres et al. 2008), R Coronae Australis association (R CrA) (Neuhäuser et al. 2000), Lower Centaurus-Crux (LCC), Octans (Torres et al. 2008), Tucana-Horologium (Tuc-Hor) (Zuckermann & Webb 2000; Torres et al. 2000; Torres et al. 2008) and Upper Scorpius (US). Furthermore, we compare our results with the ones provided by a sample of PMS and MS population in the solar neighborhood taken from the literature. A subsequent discussion on the implications of the study is presented.

## 2. Sample and observations

The 63 objects used in this study are listed in Table 1. They were selected from Torres et al. (2006) based on the following criteria: i) they have been classified as highly probable or probable member of a given association according to Torres et al. (2008); ii) they show  $v \sin i$  less than 15 km/s in order to avoid strong line blending; iii) to the best of our knowledge, they are all single stars; and iv) they are young (younger or at Pleiades age) based on the equivalent width of Li I 6708 line.

High-resolution ( $R = \frac{\lambda}{\Delta\lambda} = 50,000$  in both arms) spectroscopic observations carried out between March and September 2007 were performed using the DIC#1 390+580 mode with the UVES spectrograph (Dekker et al. 2000) at the VLT/UT2 8.2-m Kueyen Telescope (Paranal Observatory, ESO, Chile). The spectra obtained cover a wavelength interval from 4800 to 7000 Å with a gap between  $\sim 5755$  and 5833 Å.

Data reduction was performed with the UVES pipeline by carrying out the usual steps for echelle data reduction. For most of the targets, multiple exposures had to be taken in order to avoid saturation. Once extracted, the multiple spectra for a given target were put at rest velocity and combined to make a high SNR ( $\sim 150$ -200) final spectra.

The synthesis of the H $\alpha$  and the H $\beta$  profiles was carried out using the 2D extracted spectra (i.e., the intermediate pipeline product prior to the merging of the spectral orders). This step is necessary in order to properly normalize the regions of the Balmer profiles to the relative continuum. We refer the reader to the work of Ammler-von Eiff & Santos (2008) for a detailed explanation of the different steps of the reduction procedure.

The comparison data for MS dwarfs used in this paper were taken from Sousa et al. (2008) (hereafter SOU08) and Gilli et al. (2006) (hereafter GI06) whereas the WTTS comparison sample comes from Santos et al. (2008) (hereafter SA08).

## 3. Analysis of Spectra

### 3.1. Stellar parameters and abundances

The stellar parameters and iron abundances shown here were determined using the same methodology described in Santos et al. (2004). Preliminary work consisted in measuring the equivalent widths (EW) of a set of FeI and FeII lines on the collected spectra using the IRAF plot tool and a gaussian fitting procedure.

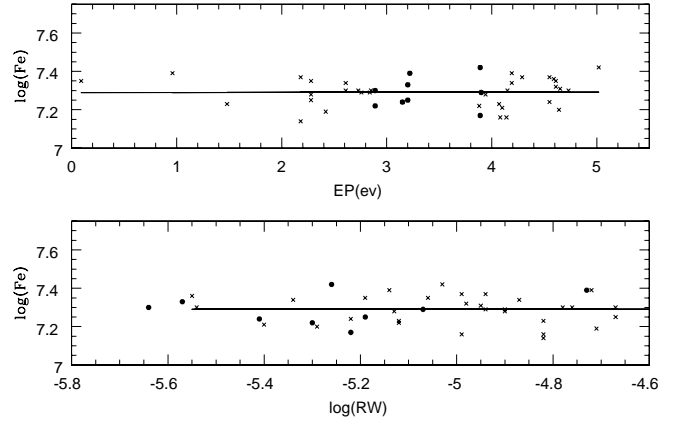


**Fig. 1.** Individual line FeI (crosses) and FeII (filled circles) abundances as a function of the excitation potential (top panel) and the reduced equivalent width,  $RW = EW/\lambda$  (bottom panel) for one of the coolest stars in the sample, CD-22 11502 in the US association. In both cases, no systematic dependence of the derived abundances is seen as a function of these two quantities.

The line list of the FeI/FeII species considered was taken from aforementioned paper and is composed essentially by weak lines with an extended range of excitation potentials in order to ensure a robust fitting.

A spectroscopic analysis was then performed with a recent version (2002) of the radiative transfer code MOOG (Snedden et al. 1973) using the local thermodynamic equilibrium (LTE), constant flux, blanketed atmospheric models, taken from the ATLAS9 stellar grid of Kurucz (1993).

The four fundamental parameters, effective temperature ( $T_{eff}$ ), surface gravity ( $\log g$ ), microturbulence ( $\xi_t$ ) and the Iron abundance ( $[Fe/H]$ ) presented here were furthermore derived by imposing the Fe excitation/ionization equilibrium.

In Fig. 1 we show an example of the two final fits (slope  $\sim 0.00$ ) obtained for a cool star (CD-22 11502) with a  $T_{eff}$  of 4951K. Of particular interest in those plots is the small dispersion of the iron abundances found.

The errors affecting the parameters were computed through the very same method as in Gonzalez (1998). Final derived parameters, abundances, and uncertainties are presented in Table 2. We should point out that the errors displayed in this study only represent relative uncertainties. They do not assert absolute uncertainties on the atmospheric parameters but rather underlying errors stacked to the method used in this study.

In addition to Iron, abundances for Si and Ni were also derived. We refer the reader to the papers of Santos et al. (2006) and GI06 for a description of the procedures and atomic line list used. Resulting abundances and errors for these elements are given in Table 5. Furthermore, abundance ratios  $[X/Fe]$  (with  $X = Ni$  and  $Si$ ) were compared with those from GI06, who applied the same method, line list and atmospheric models.

All abundances displayed here are differential with respect to the Sun. The following solar parameters were adopted:  $T_{eff} = 5777$  K,  $\log g = 4.44$  dex,  $\xi_t = 1.00$  km s $^{-1}$ ,  $\log \epsilon_{Fe} = 7.47$  dex. Solar abundances for these for Si and Ni were taken from Anders & Grevesse (1989).

Similarly to previous studies on PMS stars (Padgett 1996; James et al. 2006; Santos et al. 2008), the microturbulence val-

**Table 3.** Average Fe abundances and standard deviations found in each association. If only one star is studied the  $\sigma$  displayed comes from the determination of its  $[\text{Fe}/\text{H}]$ . The average values of  $[\text{Fe}/\text{H}]$  found in the stellar sample of SA08 and SOU08 are also shown. The columns marked with an asterisk are the corrected average  $[\text{Fe}/\text{H}]$  and the new  $\sigma$  computed according to the method presented in section 3.2.

Association	$\langle[\text{Fe}/\text{H}]\rangle$	$\sigma$	$\langle[\text{Fe}/\text{H}]\rangle^*$	$\sigma^*$	$N_{\text{stars}}$
AB Dor	-0.01	0.09	0.04	0.05	12
Argus	-0.03	0.05	0.02	0.06	7
$\beta$ Pic	-0.13	0.08	-0.01	0.08	1
Carina	-0.07	0.04	0.01	0.04	7
Columba	-0.05	0.07	-0.03	0.07	6
R CrA	-0.08	0.00	0.00	0.00	2
$\epsilon$ Cha	0.01	0.05	0.03	0.05	1
LCC	-0.06	0.05	0.02	0.05	7
Octans	-0.09	0.06	-0.03	0.05	1
Tuc-Hor	-0.06	0.09	-0.03	0.05	9
US	-0.11	0.10	-0.02	0.09	10
Total sample	-0.06	0.08	0.00	0.06	63
SA08	-0.08	0.09	0.04	0.06	28
SOU08	-0.10	0.24	-	-	450

ues obtained for the PTTS studied here are somewhat higher than the typical ones usually exhibited by MS field dwarfs. The reason for these larger values is unknown. It has been suggested that this may be caused by an enhanced magnetic field activity known to be considerably stronger during the pre-main sequence phase (SA08).

We plotted the microturbulence against the various parameters involved in the determination, such as the  $T_{\text{eff}}$ ,  $\log g$ ,  $[\text{Fe}/\text{H}]$ , and  $\nu \sin i$  in order to detect possible trends which could be at the origin of these higher microturbulence values. Despite a smooth dependence on the temperature, the cooler the star the higher the  $\xi_t$ , it seems that there is no apparent influence of other factors such as the  $\nu \sin i$  of the stars. In this context, we were not able to understand whether these results come from the intrinsic physics of the stars studied here or, for instance, from the atmospheric models used.

### 3.2. $[\text{Fe}/\text{H}]$ correction

Inspecting the atmospheric parameters and Fe abundances shown in Table 2 we note that in the temperature range from 4500K to 5500K the determined values of  $[\text{Fe}/\text{H}]$  suffer an overall increase as a function of  $T_{\text{eff}}$  (Fig. 2). This fact is true for any given association studied. Overplotting the  $[\text{Fe}/\text{H}]$  and  $T_{\text{eff}}$  derived by SA08 to our own values we promptly see that the trend reported by these authors is similar to the one found in our analysis.

The trend shown in Figure 2 contradicts the standard idea that stars originated within the same cloud will show a similar abundance pattern. Therefore, we believe that the slope seen in Fig. 2 is likely to be due to systematic errors. In this respect, it is known that PMS stars often display an enhanced stellar activity and the spectroscopic results, like atmospheric parameters, may become modulated by stellar spots, strong magnetic

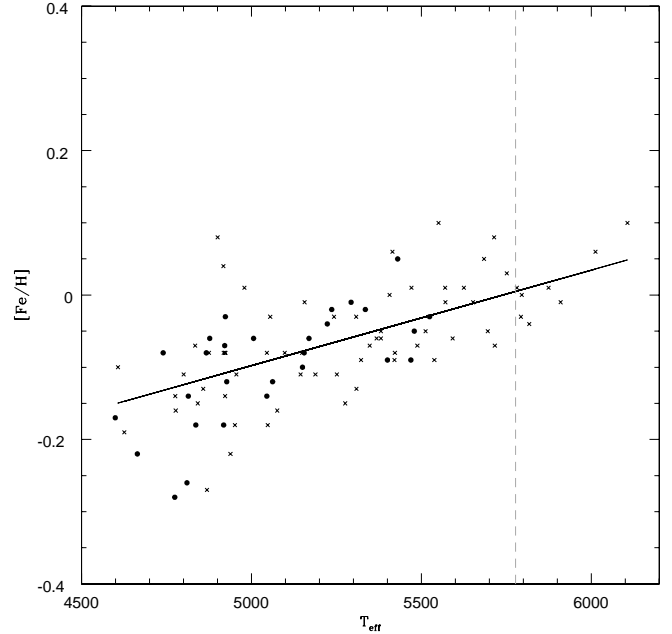


**Fig. 2.**  $T_{\text{eff}}$  vs  $[\text{Fe}/\text{H}]$  plot for the stars studied in this work (crosses) and that of SA08 (filled circles). The solid black line represents a simple least square fit of the initial values found. The slope of the line is of about 0.13dex per 1000K. The dashed vertical line represents the solar value used as a reference.

fields or NLTE effects. Moreover, as the star gets cooler, the line blending becomes stronger, causing a possible  $[\text{Fe}/\text{H}]$  underestimation. An extensive study of the influence of stellar spots on deriving stellar parameters can be found, for instance, in Morel et al. (2004).

A possible influence of the atmospheric models used, optimal in the temperature window considered, cannot be discarded. However, tests carried out in Sec. 3.3 (see below) do not support such hypothesis. A robust comparison sample with different stellar models is needed in order to understand if the trend observed is a by-product of the analysis employed or if it has a real origin in the stars studied.

Regardless the origin of this effect, a first-order correction was carried out by performing a simple linear least square fit to the data points in Fig 2. We then subtracted from all  $[\text{Fe}/\text{H}]$  values the fitted relation, assuming that for the solar temperature no correction was needed. The same correction was applied for the SA08 metallicities. The  $[\text{Fe}/\text{H}]$  values corrected by this method are shown in the asterisked columns in Table 2 and Table 3.

By looking at the corrected results in these two tables we see that a slightly smaller dispersion within each association is found. However, since we cannot find a physical justification for the correction applied above, only the original (uncorrected) values of  $[\text{Fe}/\text{H}]$  obtained were considered throughout the paper.

### 3.3. $H\alpha$ and $H\beta$ synthetic profiles

To further establish the consistency of the stellar parameters, and more specifically of  $T_{\text{eff}}$  as determined using the method described in section 3.1, we computed the synthetic profiles for the two Balmer lines,  $H\alpha$  and  $H\beta$ . It has been shown that H-line profiles are very sensitive to temperature variations, but quite insensitive to gravity and metallicity variations (see e.g. Fuhrmann

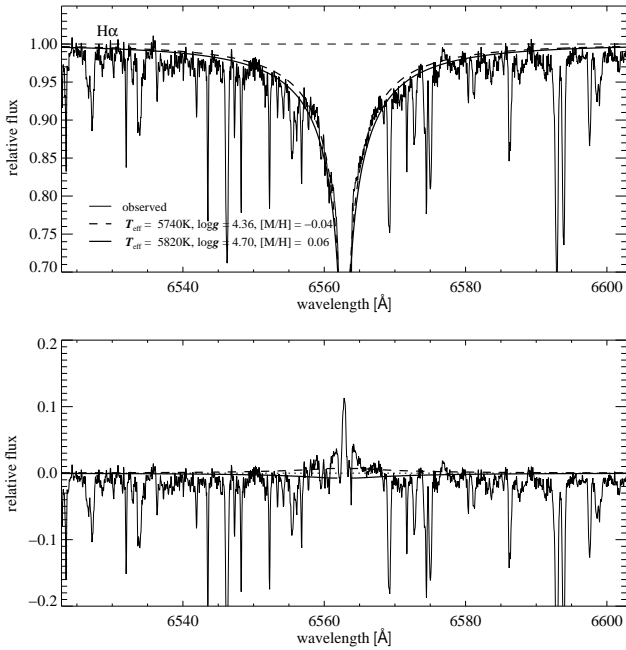


**Fig. 3.** Observed and synthetic  $H\alpha$  profile for the star HD47875. The horizontal dashed line represents the assumed continuum. One profile was computed for a lower limit (dashed line) on all parameters and another for an upper limit (solid line). The residuals of the yielded comparison are displayed in the lower panel.

et al. 2004 and references therein). That is the reason why it is possible to derive quite accurate stellar  $T_{eff}$  from the hydrogen lines.

Ten stars of the whole sample were used, half of them featured in our analysis as having  $T_{eff}$  lower than the Sun and the other half with approximately solar  $T_{eff}$ .

The profiles were calculated with the LINFOR line formation code using the MAFAGS model atmospheres as described in Fuhrmann et al. (2004 and previous papers), Ammler (2006), Ammler-von Eiff & Santos (2008). We then compared the synthetic profiles with those observed in the stellar spectra. The method used consisted in picking the  $T_{eff}$ ,  $\log g$ ,  $\xi_t$  and the  $[Fe/H]$  in Table 2 to derive two profiles for both the  $H\alpha$  and  $H\beta$  lines for each star in the sample. One profile is calculated for the lower limits on all parameters and one for the upper limits on all parameters given by the uncertainty range on the parameters in Table 2. This is a good choice since reducing  $\log g$  and  $[Fe/H]$  has the same effect on the profiles as reducing  $T_{eff}$ , which maximizes the effect of the uncertainties onto the synthetic profiles.

Note that the comparison of the synthetic profiles to the observed profiles is only valid down to relative flux levels of about 70 percent. Below this value, deviation due to NLTE starts to play a role Fuhrmann et al. (2004 and previous papers).

For some stars, the  $H\alpha$  lines seemed strongly affected by chromospheric emission, the strongest displayed by CD-361785. The  $H\beta$  seems less affected throughout the whole sample. We decided to probe the influence of this emission on the Balmer line wings and implications for derivation of effective temperature by computing the residuals as displayed in the lower panel of Fig 3.

In this plot, the limiting synthetic profiles were not subtracted from the observed profile. Instead, an additional synthetic profile was calculated based on the nominal stellar parameters (regardless of the error bars). This synthetic profile then was subtracted from the limiting synthetic profiles as well as from

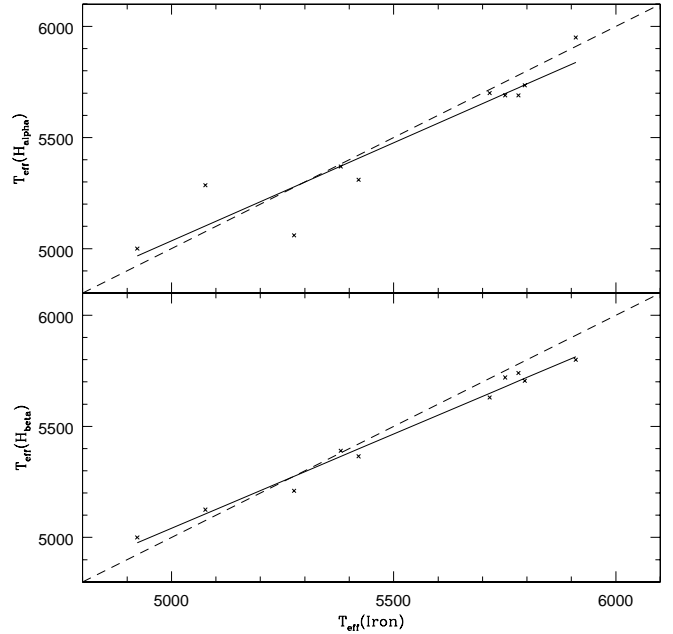


**Fig. 4.** Comparison between effective temperatures derived using iron lines with those obtained through synthesis of the line profiles of  $H\alpha$  and  $H\beta$ . Both solid lines represent linear least square fits performed to the data (with a slope of  $\sim 0.9$ ). For clarity we also show the ideal 1:1 relation (dashed line).

the observed profile. These differences are shown in the lower panel of Fig 3.

By studying these residuals it turned out that for the chromospherically active stars  $H\beta$  seemed a better choice for confirming effective temperature. However there are usually many lines in the  $H\beta$  region and the wings cannot be properly traced. Still  $H\beta$  can be used to confirm  $T_{eff}$  when  $H\alpha$  becomes useless, e.g. in the example of CD-361785.

In the two panels of Fig 4 we plot the effective temperatures obtained through the iron excitation/ionization equilibrium against those derived by the synthesis of the  $H\alpha$  and  $H\beta$  line profiles. No clear (and strong) systematic difference is seen between the  $T_{eff}$  derived by the two methods in the temperature range covered by the stars studied in this paper. It is, therefore, wise to claim that the relation seen in Fig 4 can be extended to the whole 63 stars considered in this study.

As a conclusion we may assume that the temperatures derived using the analysis of the FeI and FeII lines agree reasonably well with those coming from the fitting of the H-line profiles (with the exception of the star CD-361785) even though in the case of the latter method another set of model atmospheres and another line formation code was used. A small systematic temperature difference may be present in the data, though not higher than  $\sim 100$  K peek to peek. Such difference could account for no more than  $\sim 0.06$  dex in the derived iron abundances (propagating the error in the temperature), and cannot thus fully explain (by a factor of 2) the  $[Fe/H]$  trend observed in Fig 2.

We should note, however, that we are considering the effective temperatures derived using H-line profiles as reference. These values are likely also not free from systematic errors, that could arise from e.g. higher difficulties to place the continuum for the lower temperature stars, or from the filling-in of the profile for the very active stars.

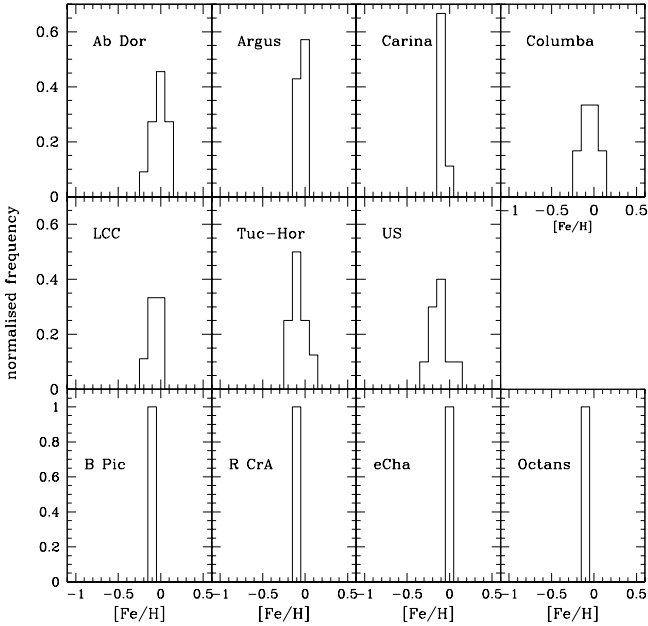


**Fig. 5.** Weighted distribution of our PTTS sample as a function of  $[Fe/H]$  for each association studied.

### 3.4. Astrometric Gravities

In addition to the test performed to the effective temperatures, we checked if there was any particular difference between our stellar gravities and those obtained through equation 1 in Santos et al. (2004), using Hipparcos parallaxes (ESA 1997), hence accurate luminosities and  $T_{eff}$ , which enable mass estimation using evolutionary tracks.

We should first stress that any conclusion yielded by this comparison should be taken with caution. The variability of the PTTS analysed, the uncertainties attached to PMS evolutionary tracks used for mass estimation are amongst some of the reasons why we must be careful in addressing stellar parameters coming from evolutionary stellar models. Indeed, stars in this phase of evolution are experiencing considerable structure contraction which can drive radius, age and mass estimations completely off the course. At the same time, Hipparcos parallaxes are not always sufficient to perform a whole sample comparison (in some cases the uncertainties are quite high).

Notwithstanding these considerations, we searched for parallax ( $\pi$ ) information in the Hipparcos catalogue to compute stellar astrometric masses that could be used for the gravity comparison. Unfortunately, from the 63 stars of Table 2 only 19 featured the catalogue. A whole sample comparison between the gravities achieved through the two different techniques was therefore not feasible.

Regardless of this, we estimated the mass for these 19 stars by using the isochrones of Shaller et al. (1992) and Shaerer et al. (1992, 1993) when interpolating the V absolute magnitudes of Table 1 with the  $T_{eff}$  of Table 2 in the resulting Hertzsprung-Russel diagram. For the Bolometric Correction we used the calibration by Flower (1996).

A comparison of the two sets of surface gravities has shown that the parallax based values are, on average, higher than the ones derived through the use of FeI and FeII lines. The average offset is of about  $\sim 0.46$  dex, with an rms of 0.32 dex. The values

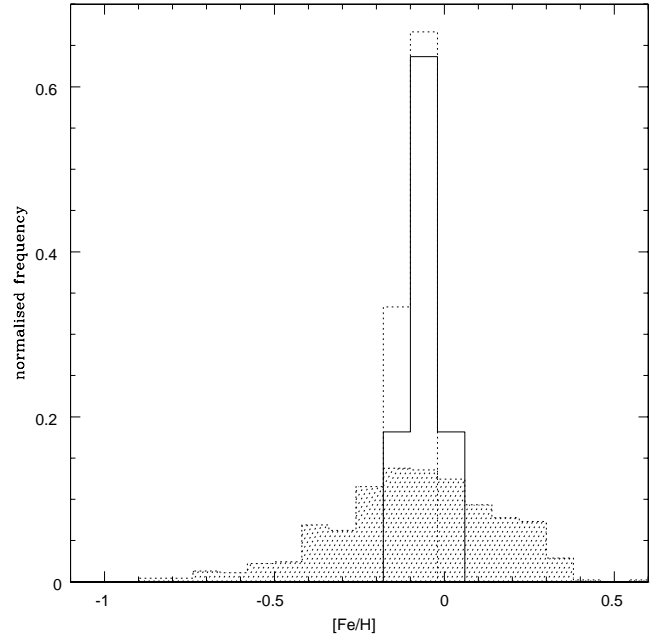


**Fig. 6.** Metallicity weighted distribution of the 6 SFR (dotted line) studied by SA08, of our 11 associations (solid line) and of the 450 MS stars (shaded area) in the solar neighborhood plotted as functions of  $[Fe/H]$ .

derived using Hipparcos gravities for the 19 stars (average of 4.80 dex) are clearly strongly above the expectation, while those derived by the method described in Sect. 3.1 (average of 4.33 dex) are usually within the expected range of values.

## 4. Results

### 4.1. Fe abundance and atmospheric parameters

By analysing the metallicity values of the different stars and the relatively small dispersions obtained (Table 2) we see that the trend described in section 3.2 rather than limiting the conclusions, it strengthens the notion that the metallicities of all associations studied here have approximately the same value, namely, around solar (Fig 5). The typical standard deviations are within the uncertainty range of the  $[Fe/H]$  determinations.

In Figure 6 the normalized distributions of the average values of  $[Fe/H]$  for the 11 associations of our sample, and for two comparison samples from SA08 and SOU08 are shown. As we can see in this Figure and also in Table 4, low dispersion values (at the level of individual errors) are also found if the dispersion of the average metallicity of all 11 associations studied in this paper and the SFRs analysed by SA08 are considered.

A striking feature of Figure 6 is that while the MS population show a broad distribution of metallicities spanning over more than 1.0 dex, the PMS sample of SA08 and the nearby young associations overlap almost entirely. Both distributions could be combined without increasing the dispersion in the final  $[Fe/H]$  distribution.

In summary, *the nearby young associations and the SFRs share the same metallicity. Within the errors, both show solar metallicities with very little (below 0.1 dex) dispersion around the mean  $[Fe/H]$  value.* Although the exact formation mecha-

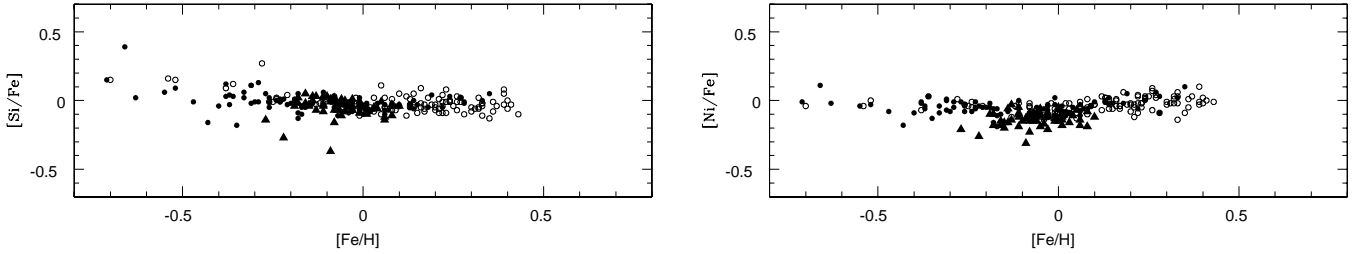


**Fig. 7.**  $[X/Fe]$  vs  $[Fe/H]$  for the PTTS in the sample (filled triangles) and for two comparison sets of stars with (open circles) and without planetary-mass companions (filled circles) in the solar neighborhood from the literature.

nism of these young associations is not known, our result is another evidence suggesting that they are somehow all related to the nearby SFRs (Torres et al. 2008). Our results brings further support to the idea suggested by SA08 that super metal-rich stars (with metallicity clearly above solar) found in the solar vicinity may have been formed in inner Galactic disk regions.

#### 4.2. Other elements

Several abundance surveys across the Galaxy over the years have shown that structural components of the Milky-Way (bulge, thin and thick disk and halo) present characteristic abundance patterns for  $\alpha$ -elements and iron-peak elements with respect to Iron and Oxygen (see e.g. McWilliam 1997; Nissen et al. 2000; Ortega et al. 2002; Fullbright 2002; Bensby et al. 2003).

In this sense, we have derived nickel (iron-peak element) and silicium ( $\alpha$ -element) abundances for the stars studied in this paper. As in SA08, we choose these two elements because the list of spectral lines used is not considerably affected by non-LTE effects. The derived abundances are given in Table 5. Additionally, the average abundance  $[X/H]$  of all the sample along with the standard deviations and the average number of spectral lines used for each species within each studied association is also given in Table 6.

In Fig. 7 we compare our results with those from GI06 for a sample of stars with and without planetary-mass companions in the solar neighborhood. Because Fe is believed to be a good indicator of the evolutionary state of an association it is extremely useful to plot  $[X/Fe]$  against  $[Fe/H]$  as it sets a plane where we can compare our results with previous studies taking this element as a reference. From Fig. 7 we can see that the abundance ratios of Si and Ni agree reasonably well with the ratios displayed by the comparison samples. In fact, in the range of  $[X/Fe]$  ratios covered by our sample, there is almost an entire overlap of the data points of the two studies.

In contrast to the Si, the nickel abundances disagree slightly from the main trend shown by the comparison sample. Our re-

**Table 4.** Weighted average of the Fe abundance and standard deviation for all the associations in our sample (Total) and for the sample of SA08 before and after correction (asterisked columns).

Sample	$\langle [Fe/H] \rangle$	$\sigma$	$\langle [Fe/H] \rangle^*$	$\sigma^*$	$N_{SFR}$
Total	-0.06	0.04	0.00	0.03	11
SA08	-0.08	0.03	0.06	0.03	6

**Table 6.** Average  $[X/H]$  abundance, corresponding standard deviation and average number of lines used for abundances determination.

Species	$\langle [X/H] \rangle$	$\sigma$	$\langle N \rangle$
Si	-0.11	0.1	8.4
Ni	0.01	0.10	23.3

sults are marginally lower than the ones obtained for MS stars by GI06. At this point, we cannot find an explanation for this small discrepancy. It might reflect simply small systematic errors in the analysis.

As concluded by SA08 for the nearby SFRs, our results show that no clear differences exist between the abundance ratios of the studied associations and those of field stars of the same metallicity. The chemical abundances for the combined young sample (SFRs from SA08 and the young associations of this paper) seem to reflect those of typical thin disk stars.

## 5. Conclusions

In this work, we have determined precise abundances for iron, silicium and nickel for 63 stars belonging to nearby young associations. While the main aim of this study was to search for a high metallicity sample within these associations, we were unable to detect any metal over-abundance in the combined sample of young stars (from this paper and those from SA08) where  $[Fe/H]$  has been derived.

Because both groups of WTTS and PTTS of the two samples have not experienced significant spatial displacements, our results imply that the high-metallicity stars harboring planets were not formed in the solar neighborhood but were instead carried to their present position by the galactic dynamical forces.

The Ni and Si abundances derived here are compatible with the general trend observed for the thin disk stellar population.

*Acknowledgements.* PVA and JFG were financially supported by the FCT project PTDC/CTE-AST/65971/2006. NCS would like to thank the support from Fundação para a Ciência e a Tecnologia, Portugal through programme Ciência 2007 (C2007-CAUP-FCT/136/2006). MAve is supported by an individual fellowship (reference SFRH/BPD/26817/2006) granted by the Fundação para a Ciência e a Tecnologia (FCT), Portugal. MAve would like to thank Klaus Fuhrmann who supplied software and model atmospheres for the analysis of the Balmer lines. Furthermore Andreas Korn is thanked for providing a program for the co-addition of spectra.

## References

Anders. E., & Grevesse, N. 1989, *Geochim, Cosmochim. Acta*, 53, 197

- Ammler M. 2006, PhD thesis, university of Jena
- Ammler - von Eiff, M. & Santos, N.C. 2008, AN, 329, 573
- Barrado y Navascués, D. 1998, Ap&SS, 263, 235
- Bensby, T., Feltzing, S. & Lundström, I. 2003, A&A, 410, 527
- Clayton, D.D., Nittler, L.R. 2004 in Origin and Evolution of the Elements, Ed. McWilliam, A., Rauch M. (Cambridge University Press), 297
- Dekker, H., D' Odorico, S., Kaufer, A., Delabre, B., & Kotzlowski, H. 2000, SPIE, 4008, 534
- ESA 1997, The Hipparcos and Tycho Catalogues, ESA SP-1200
- Feigelson, E.D., Montmerle, T. 1999 ARAA, 37, 363
- Fischer, D. & Valenti, J. 2005, ApJ, 622, 1102
- Flower, P. J. 1996, ApJ, 469, 355
- Fuhrmann, K. 2004, Astron. Nachrichten, 325, 3
- Fulbright, J. P. 2002, AJ, 123, 404
- Gilli, G., Israelian, G., Ecuivillon, A., Santos, N.C., Mayor, M. 2006, ApR, 449, 723
- Gonzalez, G. 1997, MNRAS, 285, 403
- Gonzalez, G. 1998 A&A, 334, 221
- Gonzalez, G., Laws, C., Tyagi, S., & Reddy, B. E. 2001, AJ, 121, 432
- Gregorio-Hetem, J., Lepine, J. R. D., Quast, G. R., Torres, C. A. O., de La Reza, R. 1992, AJ 103, 549
- Herbig, G.H. 1978 in Problems of Physics and Evolution of the Universe, ed. Mirzoyan L.V. (Erevan:Armenian Acad. Sci.), 171
- James, D.J., Melo, C., Santos, N.C., Bouvier, J. 2006, A&A, 446, 971
- Kasting, J. F. and Catling, D. 2003, ARAA, 41, 429
- Kastner, J.H., Zuckerman, B., Weintraub, D.A., Forveille, T. 1997, *Science*, 277, 67
- Kurucz, R. 1993, ATLAS9 Stellar Atmosphere Programs and 2 km/s grid. Kurucz CD-ROM No. 13, Cambridge, Mass.: Smithsonian Astrophysical Observatory, 1993, 13
- Mamajek, E.E., Lawson, W.A., Feigelson, E.D. 1999, ApJ, 516, 77
- Mamajek, E.E., Lawson, W.A., Feigelson, E.D. 2000, ApJ, 544, 356
- McWilliam, A., 1997, ARA&A, 35, 503
- Morel, T., Micela, G., F., & Katz, D. 2004, A&A, 426, 1007
- Neuhäuser, R. and Walter, F. M. and Covino, E. and Alcalá, J. M. and Wolk, S. J. and Frink, S. and Guillout, P. and Sterzik, M. F. and Comerón, F. 2000 A&AS, 146, 323
- Nissen, P.E., Chen, Y.Q., Shuster, W.J., & Zhao, G. 2000, A&A, 353, 722
- Ortega, V. G., de la Reza, R., Jilinski, E., Bazzanella 2002, ApJ, 575, L75
- Padgett, D.L. 1996, ApJ, 471, 847
- Pollack, J. B., Hubickyj, O., Bodenheimer, P., Lissauer, J. J., Podolak, M., Greenzweig, Y. 1996, Icarus 124, 62
- Santos, N. C., Israelian, G., & Mayor, M. 2001, A&A, 373, 1019
- Santos, N.C., Israelian, G., & Mayor, M. 2004, A&A, 415, 1153
- Santos, N. C., Israelian, G., Mayor, M., et al. 2005, A&A, 437, 1127
- Santos, N.C., Ecuivillon, A., Israelian, G., et al. 2006, A&A, 458, 997
- Santos, N.C., Melo, C., James, D.J., Gameiro, J.F., Bouvier, J., Gomes J.I. 2008, A&A, 480, 889
- Schaerer, D., Meynet, G., Maeder, A., et al. 1992, A&AS, 98, 523
- Schaller, G., Schaerer, D., Meynet, G., & Maeder, A. 1992, A&AS, 96, 269
- Schaerer, D., Charbonnel, C., Meynet, G., et al. 1993, A&AS, 102, 339
- Snedden, C. 1973, PhD. Thesis, Univ. of Texas
- Song, I., Zuckermann, B., Bessel, M.S. 2003, ApJ, 599, 342
- Sousa, S.G., Santos, N.C., Mayor, M., Udry, S., Casagrande, L., Israelian, G., Pepe, F., Queloz, D., Monteiro, M. J. P. F. G 2008, A&A, 487, 373
- Spangler, C., Sargent, A.I., Silverstone, M.D., Becklin, E.E., Zuckerman, B. 2001, ApJ, 555, 932
- Torres, C.A.O., Quast, G.R., de La Reza, R., Jilinsky, E. 2000, AJ, 120, 1410
- Torres, C.A.O., Quast, G.R., de La Reza, R., da Silva, L., Melo, C.H.F., Sterzik, M. 2003b in Open Issues in Local Star Formation, ed. Lépine, J. and Gregorio-Hetem, J. (Kluwer Academic Publishers), 299, 83
- Torres, C.A.O., Quast, G.R., da Silva, L., de La Reza, R., Melo, C.H.F., Sterzik, M. 2006, AAP, 460, 695
- Torres, C.A.O., Quast, G.R., Melo, C.H.F., Sterzik, M. 2008, [arXiv:astro-ph/0808.3362]
- Wielen, R., Fuchs, B., & Dettbarn, C. 1996, A&A, 314, 438
- Zuckermann, B., Webb, R.A. 2000, Apj, 535, 959
- Zuckermann, B., Song, I., Bessel, M.S., & Webb, R.A. 2001a, ApJ, 562, L87
- Zuckerman, B., and Song, I. 2004, ARA&A, 42, 685
- Zuckerman, B., Song, I., Bessell, M.S. 2004c, ApJ, 613, L65

**Table 1.** Stellar objects used in this study, their coordinates, V magnitude and the projected rotational velocity  $v \sin i$ . High probability members proposed for the different associations are identified with an H in the last column. The remaining stars are possible members (P).

Star	RA ( $\alpha_{2000}$ )	DEC ( $\delta_{2000}$ )	V (mag)	$v \sin i$ [km s <sup>-1</sup> ]	P.
AB Dor Association					
CD-12 243	01 20 32.3	-11 28 04	8.43	3	H
CD-40 1701	05 02 30.4	-39 59 13	10.57	6	H
HD 37572	05 36 56.9	-47 57 53	7.84	9	H
HD 37551A	05 37 12.9	-42 42 56	9.55	5	H
HD 37551B	05 37 13.2	-42 42 57	10.65	5	H
CD-34 2676	06 08 33.9	-34 02 55	10.17	13	H
CD-84 80	07 30 59.5	-84 19 28	9.96	4	H
HD 64982	07 45 35.6	-79 40 08	8.96	14	H
TYC 8243 2975 1	12 30 29.6	-52 22 27	12.04	5	P
HD 207278	21 48 48.5	-39 29 09	9.66	9	H
HD 217343	23 00 19.3	-26 09 14	7.49	12	H
HD 218860A	23 11 52.1	-45 08 11	8.75	6	H
Argus Association					
CD-29 2360	05 34 59.2	-29 54 04	10.64	11	P
CD-28 3434	06 49 45.4	-28 59 17	10.38	6	H
CD-42 2906	07 01 53.4	-42 27 56	10.61	10	H
TYC 8561 0970 1	07 53 55.5	-57 10 07	11.50	5	H
BD-20 2977	09 39 51.4	-21 34 17	10.22	10	H
CD-39 5833	09 47 19.9	-40 03 10	10.89	10	H
CD-52 10232	22 39 30.3	-52 05 17	10.85	8	H
$\beta$ Pic Association					
HD 322990	17 16 07.7	-37 28 27	11.46	10	P
Carina Association					
TYC 8862 0019 1	02 58 04.0	-62 41 14	11.67	7	P
HD 44627	06 19 12.9	-58 03 16	9.13	11	H
TYC 9178 0284 1	06 55 25.2	-68 06 21	11.91	11	P
HD 55279	07 00 30.5	-79 41 46	10.11	9	H
CD-57 1709	07 21 23.7	-57 20 37	10.72	11	H
CD-55 2543	09 09 29.4	-55 38 27	10.20	13	H
HD 298936	10 13 14.8	-52 30 54	9.79	9	P
Columba Association					
HD 26980	04 14 22.6	-38 19 02	9.08	13	H
HD 27679	04 21 10.3	-24 32 21	9.43	11	H
CD-36 1785	04 34 50.8	-35 47 21	10.84	8	H
HD 32372	05 00 51.9	-41 01 07	9.50	7	H
HD 274561	05 28 55.1	-45 34 58	11.45	7	H
CD-40 2458	06 26 06.9	-41 02 54	10.00	12	H
R CrA Association					
CD-37 12759	18 39 05.3*	-37 26 22	10.98	9	H
CD-36 13163	18 57 20.8*	-36 43 01	11.04	10	H

Star	RA ( $\alpha_{2000}$ )	DEC ( $\delta_{2000}$ )	V (mag)	$\nu \sin i$ [km s $^{-1}$ ]	P.
$\epsilon$ Cha Association					
HD 105923	12 11 38.1	-71 10 36	9.16	12	H
LCC Association					
CP-52 5025	11 55 57.7	-52 54 01	11.00	6	H
CD-49 4947	12 12 11.2	-49 50 08	11.37	14	H
CP-64 1859	12 19 21.6	-64 54 10	9.87	13	P
CD-51 6900	12 40 46.6	-52 11 05	11.91	14	H
CD-40 7581	12 56 12.3	-41 22 20	11.73	13	H
CD-40 8031	13 37 57.3	-41 34 42	10.12	13	H
CP-66 2366	13 54 07.4	-67 33 45	10.93	11	P
Octans Association					
HD 23208	03 42 39.8	-20 32 44	9.16	10	P
Tuc-Hor Association					
HD 105	00 05 52.5	-41 45 11	7.53	12	H
HD 987	00 13 53.0	-74 41 18	8.78	7	H
HD 8558	01 23 21.3	-57 28 51	8.51	14	H
HD 9054	01 28 08.7	-52 38 19	9.07	4	H
CD-46 1064	03 30 49.1	-45 55 57	9.55	10	H
HD 47875	06 34 41.0	-69 53 06	9.17	11	P
CD-38 4458	08 26 10.0	-39 02 05	10.31	9	P
HD 202917	21 20 50.0	-53 02 03	8.69	14	H
HD 222259B	23 39 39.3	-69 11 40	9.84	14	H
US Association					
CD-34 10180	15 07 14.8	-35 05 00	10.53	13	H
CD-36 10208	15 29 47.3	-36 28 37	11.16	14	H
TYC 9034 0968 1	15 33 27.5	-66 51 25	10.99	5	H
CD-39 10162	15 47 41.8	-40 18 27	11.08	12	H
CD-25 11330	16 05 50.6	-25 33 14	10.93	8	H
CD-22 11502	16 19 34.0	-22 28 29	11.11	12	H
CD-51 10295	16 33 50.4	-51 19 01	10.75	4	H
CD-31 13486	17 02 27.8	-32 04 36	10.13	13	H
CD-23 13281	17 16 18.1	-23 10 47	10.97	14	H
TYC7886 1894 1	17 58 31.5	-37 43 03	11.62	5	H

**Table 2.** Results from the spectroscopic analysis - The determined atmospheric parameters  $T_{eff}$ ,  $\log g$ ,  $[Fe/H]$ ,  $\xi_t$  for each star. In the last three columns are shown the number of Fe lines used in each determination, the average uncertainty on the abundances given by each line EW.  $[Fe/H]^*$  is the Iron abundance corrected according to the method explained in section 3.2.

Star	$T_{eff}$ [K]	$\log g$ [ $\text{cm s}^{-2}$ ]	$\xi_t$ [ $\text{km s}^{-1}$ ]	[Fe/H]	[Fe/H]*	N (FeI, FeII)	$\sigma$ (FeI, FeII)
AB Dor Association							
CD-12 243	5406±38	4.67±0.09	1.21±0.02	0.00±0.05	0.04	37, 10	0.05, 0.03
CD-40 1701	4800±80	4.61±0.24	1.68±0.14	-0.11±0.08	0.01	36, 8	0.08, 0.10
HD 37572	5251±43	4.45±0.11	1.82±0.07	-0.11±0.06	-0.05	34, 6	0.05, 0.05
HD 37551A	5684±32	4.52±0.07	1.46±0.05	0.05±0.04	0.06	33, 12	0.04, 0.03
HD 37551B	5055±68	4.31±0.14	1.65±0.08	-0.03±0.08	0.06	36, 8	0.07, 0.06
CD-34 2676	5571±86	4.47±0.20	2.08±0.14	-0.01±0.10	0.01	32, 8	0.08, 0.08
CD-84 80	5381±45	4.53±0.16	1.53±0.07	-0.05±0.05	0.00	38, 12	0.05, 0.07
HD 64982	6106±72	4.14±0.30	1.53±0.13	0.10±0.09	0.05	32, 12	0.07, 0.12
TYC 8243 2975 1	4626±74	4.16±0.22	1.35±0.11	-0.19±0.07	-0.04	31, 6	0.07, 0.09
HD 207278	5714±52	4.51±0.10	1.45±0.08	0.08±0.06	0.08	33, 9	0.05, 0.05
HD 217343	5795±41	4.44±0.09	1.68±0.08	0.00±0.05	-0.01	34, 10	0.04, 0.05
HD 218860A	5550±68	4.50±0.13	1.42±0.05	0.10±0.06	0.13	34, 12	0.05, 0.05
Argus Association							
CD-29 2360	4917±77	4.66±0.16	1.92±0.12	0.04±0.07	0.15	32, 5	0.08, 0.06
CD-28 3434	5652±39	4.51±0.13	1.62±0.07	-0.01±0.05	0.00	35, 11	0.04, 0.06
CD-42 2906	5308±49	4.38±0.13	1.76±0.07	-0.03±0.07	0.03	36, 8	0.06, 0.06
TYC 8561 0970 1	5348±51	4.48±0.15	1.75±0.07	-0.07±0.07	-0.02	38, 12	0.06, 0.06
BD-20 2977	5421±50	4.50±0.14	2.05±0.09	-0.09±0.06	-0.05	33, 10	0.05, 0.07
CD-39 5833	5471±61	4.45±0.12	1.72±0.10	0.01±0.07	0.05	35, 9	0.07, 0.05
CD-52 10232	5381±59	4.48±0.13	1.83±0.09	-0.06±0.07	-0.01	35, 10	0.07, 0.06
$\beta$ Pic Association							
HD 322990	4858±74	4.20±0.20	2.05±0.10	-0.13±0.08	-0.01	31, 9	0.08, 0.10
Carina Association							
TYC 8862 0019 1	4776±120	4.38±0.47	2.29±0.2	-0.14±0.14	-0.01	38, 10	0.14, 0.25
HD 44627	5156±54	4.29±0.17	1.90±0.06	-0.01±0.06	0.07	30, 8	0.05, 0.08
TYC 9178 0284 1	4607±89	3.98±0.36	1.90±0.12	-0.10±0.08	0.05	28, 6	0.08, 0.19
HD 55279	4918±50	4.19±0.18	1.85±0.07	-0.08±0.05	0.03	33, 8	0.05, 0.08
CD-57 1709	5368±55	4.58±0.19	1.85±0.08	-0.06±0.06	-0.01	33, 10	0.05, 0.09
CD-55 2543	5512±53	4.38±0.20	1.70±0.08	-0.05±0.06	-0.02	31, 8	0.05, 0.09
HD 298936	4923±119	4.47±0.29	1.96±0.14	-0.08±0.08	0.03	30, 8	0.06, 0.08
Columba Association							
HD 26980	5910±61	4.26±0.12	1.74±0.12	-0.01±0.07	-0.03	34, 10	0.07, 0.06
HD 27679	5817±58	4.16±0.31	1.96±0.13	-0.04±0.08	-0.05	37, 12	0.07, 0.14
CD-36 1785	5276±48	4.31±0.19	2.63±0.09	-0.15±0.06	-0.09	32, 7	0.05, 0.09
HD 32372	5716±50	4.31±0.09	1.89±0.10	-0.07±0.07	-0.07	38, 11	0.06, 0.04
HD 274561	5144±63	4.36±0.12	2.09±0.10	-0.11±0.07	-0.03	30, 7	0.06, 0.05
CD-40 2458	5415±62	4.32±0.19	1.98±0.09	0.06±0.08	0.1	34, 9	0.07, 0.09
R CrA Association							
CD-37 12759	5149±104	4.28±0.30	1.98±0.15	-0.08±0.13	0.00	35, 10	0.07, 0.07
CD-36 13163	5098±44	3.99±0.13	1.73±0.05	-0.08±0.06	0.00	31, 9	0.05, 0.07

Star	$T_{eff}$ [K]	$\log g$ [ $\text{cm s}^{-2}$ ]	$\xi_t$ [ $\text{km s}^{-1}$ ]	[Fe/H]	[Fe/H]*	N (FeI , FeII)	$\sigma$ (FeI , FeII)
$\epsilon$ Cha Association							
HD 105923	4979 $\pm$ 40	3.98 $\pm$ 0.13	1.94 $\pm$ 0.06	0.01 $\pm$ 0.05	0.03	32 , 8	0.05 , 0.06
LCC Association							
CP-52 5025	4834 $\pm$ 78	4.19 $\pm$ 0.18	1.69 $\pm$ 0.10	-0.07 $\pm$ 0.07	0.05	28 , 7	0.07 , 0.06
CD-49 4947	4875 $\pm$ 56	4.17 $\pm$ 0.20	2.21 $\pm$ 0.07	-0.08 $\pm$ 0.06	0.03	28 , 6	0.06 , 0.10
CP-64 1859	5422 $\pm$ 145	5.14 $\pm$ 0.25	1.46 $\pm$ 0.25	-0.08 $\pm$ 0.13	0.03	30 , 7	0.11 , 0.09
CD-51 6900	4842 $\pm$ 71	3.98 $\pm$ 0.18	2.04 $\pm$ 0.10	-0.15 $\pm$ 0.08	-0.03	29 , 4	0.07 , 0.08
CD-40 7581	4979 $\pm$ 69	4.20 $\pm$ 0.13	1.80 $\pm$ 0.08	0.01 $\pm$ 0.07	0.11	30 , 4	0.07 , 0.04
CD-40 8031	5243 $\pm$ 55	4.06 $\pm$ 0.21	1.78 $\pm$ 0.07	-0.03 $\pm$ 0.07	0.04	31 , 7	0.06 , 0.10
CP-66 2366	5793 $\pm$ 75	4.89 $\pm$ 0.34	2.15 $\pm$ 0.15	-0.03 $\pm$ 0.08	-0.04	25 , 9	0.06 , 0.15
Octans Association							
HD 23208	5322 $\pm$ 43	4.23 $\pm$ 0.14	1.85 $\pm$ 0.06	-0.09 $\pm$ 0.06	-0.03	34 , 8	0.05 , 0.07
Tuc-Hor Association							
HD 105	6012 $\pm$ 68	4.42 $\pm$ 0.12	1.24 $\pm$ 0.12	0.06 $\pm$ 0.09	0.02	36 , 8	0.07 , 0.05
HD 987	5488 $\pm$ 46	4.36 $\pm$ 0.12	1.85 $\pm$ 0.08	-0.07 $\pm$ 0.06	-0.04	35 , 11	0.05 , 0.06
HD 8558	5538 $\pm$ 53	4.04 $\pm$ 0.16	1.90 $\pm$ 0.09	-0.09 $\pm$ 0.07	-0.06	30 , 7	0.06 , 0.07
HD 9054	5045 $\pm$ 55	4.49 $\pm$ 0.15	1.90 $\pm$ 0.07	-0.08 $\pm$ 0.06	0.01	31 , 9	0.05 , 0.07
CD-46 1064	4777 $\pm$ 70	4.13 $\pm$ 0.18	1.92 $\pm$ 0.10	-0.16 $\pm$ 0.07	-0.03	33 , 6	0.07 , 0.07
HD 47875	5781 $\pm$ 35	4.53 $\pm$ 0.17	1.75 $\pm$ 0.07	0.01 $\pm$ 0.05	0.00	33 , 9	0.04 , 0.07
CD-38 4458	5751 $\pm$ 34	4.32 $\pm$ 0.11	1.60 $\pm$ 0.06	0.03 $\pm$ 0.05	0.03	35 , 10	0.04 , 0.05
HD 202917	5592 $\pm$ 79	4.31 $\pm$ 0.17	2.16 $\pm$ 0.15	-0.06 $\pm$ 0.10	-0.04	33 , 9	0.08 , 0.07
HD 222259B	4938 $\pm$ 91	4.12 $\pm$ 0.26	2.59 $\pm$ 0.15	-0.22 $\pm$ 0.09	-0.11	27 , 8	0.08 , 0.12
US Association							
CD-34 10180	5188 $\pm$ 49	4.05 $\pm$ 0.20	2.30 $\pm$ 0.08	-0.11 $\pm$ 0.07	-0.04	34 , 8	0.06 , 0.10
CD-36 10208	4869 $\pm$ 71	3.64 $\pm$ 0.23	2.59 $\pm$ 0.10	-0.27 $\pm$ 0.07	-0.16	27 , 5	0.07 , 0.11
TYC 9034 0968 1	4955 $\pm$ 65	4.52 $\pm$ 0.47	1.80 $\pm$ 0.07	-0.11 $\pm$ 0.11	-0.01	33 , 9	0.07 , 0.13
CD-39 10162	4922 $\pm$ 61	4.05 $\pm$ 0.14	2.04 $\pm$ 0.09	-0.14 $\pm$ 0.08	-0.03	33 , 7	0.07 , 0.10
CD-25 11330	5076 $\pm$ 62	4.14 $\pm$ 0.18	2.02 $\pm$ 0.09	-0.16 $\pm$ 0.07	-0.07	34 , 11	0.06 , 0.08
CD-22 11502	4951 $\pm$ 66	3.81 $\pm$ 0.17	2.10 $\pm$ 0.08	-0.18 $\pm$ 0.07	-0.08	34 , 9	0.07 , 0.08
CD-51 10295	4922 $\pm$ 58	4.31 $\pm$ 0.20	1.59 $\pm$ 0.07	-0.08 $\pm$ 0.05	0.03	31 , 6	0.06 , 0.10
CD-31 13486	5625 $\pm$ 42	4.55 $\pm$ 0.25	1.68 $\pm$ 0.07	0.01 $\pm$ 0.06	0.03	35 , 10	0.06 , 0.11
CD-23 13281	4900 $\pm$ 84	4.41 $\pm$ 0.26	2.14 $\pm$ 0.32	0.08 $\pm$ 0.17	0.19	28 , 6	0.08 , 0.10
TYC 7886 1894 1	5048 $\pm$ 62	4.26 $\pm$ 0.18	2.16 $\pm$ 0.09	-0.18 $\pm$ 0.07	-0.09	33 , 9	0.06 , 0.08

**Table 5.** Derived abundances of Si and Ni for the stars in the sample.

Star	[Si/H]	$\sigma$	$N$	[Ni/H]	$\sigma$	$N$
AB Dor						
CD-12 243	-0.05	0.03	9	-0.05	0.04	25
CD-40 1701	-0.08	0.10	7	-0.16	0.10	24
HD 37572	-0.09	0.04	9	-0.02	0.07	25
HD 37551A	0.04	0.04	9	0.02	0.06	30
HD 37551B	-0.02	0.04	9	0.02	0.07	27
CD-34 2676	-0.14	0.09	9	-0.06	0.09	20
CD-84 80	-0.05	0.04	9	-0.04	0.05	25
HD 64982	0.02	0.07	9	-0.26	0.14	22
TYC 8243 2975 1	-0.23	0.08	6	-0.10	0.18	24
HD 207278	0.05	0.03	9	0.13	0.08	27
HD 217343	-0.05	0.05	9	0.07	0.06	22
HD 218860A	0.06	0.03	9	0.1	0.07	29
Argus						
CD-29 2360	-0.02	0.09	9	-0.03	0.08	20
CD-28 3434	-0.04	0.04	9	-0.01	0.06	28
CD-42 2906	-0.07	0.07	9	0.06	0.06	26
TYC 8561 0970 1	-0.09	0.04	9	-0.01	0.06	27
BD-20 2977	-0.1	0.06	9	-0.01	0.07	22
CD-52 10232	-0.05	0.03	9	0.04	0.08	26
CD-39 5833	-0.07	0.05	9	0.08	0.07	27
$\beta$ Pic						
HD 322990	-0.1	0.13	9	0.02	0.09	23
Carina						
TYC 8862 0019 1	-0.11	0.13	8	-0.10	0.12	21
HD 44627	-0.02	0.10	9	0.10	0.09	24
TYC 9178 0284 1	-0.07	0.12	8	0.05	0.11	19
HD 55279	-0.07	0.07	9	-0.01	0.08	23
CD-57 1709	-0.09	0.07	8	0.01	0.08	24
CD-55 2543	-0.13	0.07	8	0.00	0.11	18
HD 298936	-0.08	0.11	9	-0.05	0.09	22
Columba						
HD 26980	-0.1	0.08	8	-0.16	0.06	17
HD 27679	-0.09	0.06	8	0.11	0.10	21
CD-36 1785	-0.18	0.08	9	0.06	0.08	25
HD 32372	-0.12	0.04	9	0.06	0.06	27
HD 274561	-0.15	0.07	9	0.04	0.08	25
CD-40 2458	-0.08	0.08	7	0.15	0.09	24
R CrA						
CD-37 12759	-0.09	0.08	9	0.04	0.08	22
CD-36 13163	-0.06	0.06	9	0.05	0.09	25
$\epsilon$ Cha						
HD 105923	-	-	-	-	-	-

Star	[Si/H]	$\sigma$	$N$	[Ni/H]	$\sigma$	$N$
LCC						
CP-52 5025	-0.14	0.10	8	0.10	0.09	23
CD-49 4947	-0.15	0.10	5	-0.08	0.13	15
CP-64 1859	-0.24	0.18	7	-0.13	0.13	17
CD-51 6900	-0.19	0.08	8	0.03	0.11	19
CD-40 7581	-0.09	0.11	9	0.07	0.12	24
CD-40 8031	-0.1	0.09	8	0.07	0.09	18
CP-66 2366	-0.10	0.07	7	-0.04	0.06	15
Octans						
HD 23208	-0.08	0.09	9	0.02	0.08	27
Tuc-Hor						
HD 105	-0.06	0.07	9	0.16	0.17	20
HD 987	-0.12	0.04	9	0.06	0.09	28
HD 8558	-0.46	0.31	3	-0.4	0.34	11
HD 9054	-0.09	0.08	9	-0.06	0.08	23
CD-46 1064	-0.11	0.11	9	-0.07	0.10	21
HD 47875	-0.05	0.06	9	0.14	0.11	22
CD-38 4458	-0.02	0.09	9	0.12	0.07	26
HD 202917	-0.17	0.06	8	0.05	0.17	23
HD 222259B	-0.49	0.14	6	0.00	0.17	19
US						
CD-34 10180	-0.19	0.09	8	0.1	0.12	22
CD-36 10208	-0.41	0.11	6	0.07	0.13	20
TYC 9034 0968 1	-0.14	0.11	9	-0.1	0.10	25
CD-39 10162	-0.14	0.09	9	-0.03	0.10	24
CD-25 11330	-0.18	0.06	9	-0.02	0.11	27
CD-22 11502	-0.20	0.07	8	0.04	0.11	23
CD-51 10295	-0.09	0.08	9	0.00	0.10	25
CD-31 13486	-0.04	0.04	9	0.07	0.09	25
CD-23 13281	-0.03	0.10	8	0.07	0.16	24
TYC 7886 1894 1	-0.16	0.08	9	0.09	0.16	29